Journal of
Materials Chemistry A

ROYAL SOCIETY
OF CHEMISTRY

PERSPECTIVE

View Article Online
View Journal | View Issue

Cite this: *J. Mater. Chem. A*, 2024, **12**, 33470

Evolution of small molecules as photocatalysts towards production of green hydrogen

Tumpa Gorai *[a] and Surya Prakash Singh *[ab]

Received 1st August 2024
Accepted 4th November 2024

DOI: 10.1039/d4ta05353b

rsc.li/materials-a

With the increased demand for green and sustainable sources of fuels, photocatalytic hydrogen gas production using semiconductor catalysts is attracting tremendous attention. In this perspective article, we will discuss the state-of-the-art development of small molecule-based semiconductors for photocatalytic green hydrogen production. Organic small molecules have the benefits of easy structural engineering allowing fine modulation of optical and electronic properties for the development of efficient photocatalysts. Small molecule-based photocatalyst development is advantageous compared to that of their polymer counterparts due to various reasons including less tedious synthesis, easily tunable optical and electronic properties, improved water dispersibility, *etc.* Conjugated donor–acceptor, porphyrin, perylene, and organic heterojunction nanoparticles are discussed in this article for their photocatalytic activity in the hydrogen evolution reaction. We have highlighted literature reports emphasizing the impact of heteroatom substitution, conjugation, band gap, exciton diffusion length, planarity, crystallinity, molecular packing, water solubility, *etc.* on photocatalytic performance.

1 Introduction

The demand for alternate green energy sources is increasing rapidly with the rapid depletion of fossil fuel sources and the rise in the global warming rate. Alternate renewable sources of green energy will prevent global warming and will sustain the increased energy demand.[1–6] Hydrogen with high energy density and as a carbon-free source of fuel has attracted widespread attention.[7–10] Each kilogram of hydrogen gas as a fuel contains 2.4 times as much energy as natural gas, and it burns without the production of CO_2 and NO_x gases.[11] Therefore, efficient production of hydrogen gas using green approaches will significantly prevent environmental challenges, and circumvent the energy crisis. Water is a green, inexhaustible and cheaper source of hydrogen production by water splitting. Electrocatalysis (photovoltaic-assisted electrolysis), photoelectrochemical, and photocatalysis are three different approaches for water splitting/hydrogen production by solar irradiation.[12] The photovoltaic-assisted method showed promising hydrogen production efficiency (>28%);[13] however the production cost is high for industrial-scale hydrogen fuel production. Solar energy-driven photocatalysis is a green and low-cost approach for the production of green hydrogen. Hydrogen production by splitting of water requires a photocatalyst which will absorb solar energy and achieve the required charge separation for hydrogen gas production.

The first report on solar energy driven electrochemical water splitting for hydrogen and oxygen gas evolution was by Fujishima, A. & Honda, K. in 1972 using a TiO_2 and Pt black electrode combination as a semiconductor photocatalyst.[14,15] Since then, various inorganic semiconductor based photocatalysts have been investigated for hydrogen evolution.[16–18] Transition metal complexes are also widely explored for the photocatalytic hydrogen evolution (PHE) reaction.[19] Although inorganic materials are reported for excellent hydrogen evolution reaction, there are a few drawbacks limiting their application for practical purposes, *i.e.*, the low stability under acidic conditions and fixed specific arrangement of the d orbital don't allow the tunability of the electronic energy level. Organic semiconductors such as conjugated polymers,[20–22] graphitic carbon nitride (g-C_3N_4),[23–25] covalent organic frameworks,[26,27] *etc.* were recently investigated for photocatalytic hydrogen evolution. However, difficulty in synthesis and characterisation, batch-to-batch deviation in molecular weight, porosity, and photophysical properties, limited water solubility and dispersibility, and an unclear understanding of photocatalysis mechanisms limit their application for photocatalysis.[28] The use of small molecule based photocatalysts has recently attracted attention since it drastically reduces the synthetic challenges, and the structural tunability of high photocatalytic performance is possible.

Organic small molecule semiconductors are monocyclic or polycyclic extended pi-conjugated aromatic compounds with molecular weight <1000 dalton and many structural variations.

---

[a] *Department of Polymers and Functional Materials, CSIR-Indian Institute of Chemical Technology, Hyderabad 500007, Telangana, India*

[b] *Academy of Scientific and Innovative Research (AcSIR), Ghaziabad 201002, Uttar Pradesh, India. E-mail: tumpagorai@gmail.com; spsingh@iict.res.in*

Their backbone is formed from earth-abundant carbon, and heteroatoms, *e.g.* nitrogen, oxygen, and sulfur, which makes large-scale synthesis less expensive compared to metal based photocatalysts. Organic small molecule-based photocatalysts have pi-orbital energy levels which are tunable by structural engineering, and the solubility of small molecule-based photocatalysts can also be modulated by the introduction of the required functional groups. Therefore, optical and electronic properties can be modulated by structural engineering. The reduced complexity of synthesis and less stringent reaction conditions compared to those of conjugated polymer photocatalysts allow for large-scale synthesis and isolation of small molecules with precise molecular weight and photophysical properties, which allows reproducibility of photocatalytic performance. Therefore, the development of organic small molecule based photocatalysts allows for better flexibility and tunability required for efficient photocatalytic hydrogen evolution. In this review article, we will discuss the basic principle of photocatalytic hydrogen evolution and the applicability of different kinds of small molecules as photocatalysts for green hydrogen evolution.

2 The general strategy for photocatalysis

Water splitting which involves the splitting of water molecules to produce hydrogen and oxygen, is an energy uphill reaction with the Gibbs free energy ($\Delta G°$) = 237 kJ mol^{-1}.[12] Therefore, the reaction doesn't occur spontaneously and the use of a photocatalyst accelerates the reaction rate for photocatalytic hydrogen and oxygen gas evolution. Photocatalytic hydrogen gas evolution involves consecutive steps of photophysical and redox reactions (Fig. 1).[29] Upon the absorption of photons, electrons in the valence band of the photocatalyst are excited to the conduction band with the creation of holes and excited electrons in the valence and conduction bands, respectively in the initial stage. Subsequently, the electrons and holes migrate to the surface independently, and take part in the hydrogen evolution reaction (HER) and oxygen evolution reaction (OER)

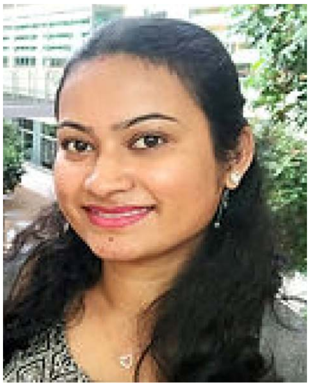

Tumpa Gorai

Dr Tumpa Gorai received her MSc degree in chemistry from the Indian Institute of Technology, Kharagpur, in the year 2011 and PhD degree from the Indian Institute of Science, Bangalore, in the year 2017. She did her initial postdoctoral research at Pohang University of Science and Technology, South Korea, and subsequently, she was an IRC Postdoctoral Fellow at Trinity College Dublin, Ireland. Currently, she is working as a DST Inspire Faculty Fellow at the Department of Polymers & Functional Materials, CSIR-IICT Hyderabad, India. Her current research interest is developing emerging supramolecular materials for photonics and sustainable development.

Surya Prakash Singh

Dr Surya Prakash Singh is currently working as a Principal Scientist at the Department of Polymers and Functional Materials, CSIR-Indian Institute of Chemical Technology, Hyderabad. Dr Singh graduated with a PhD from the University of Allahabad, India. After working at the Nagoya Institute of Technology, Japan, as a postdoctoral fellow, he joined Osaka University, in 2008 as an Assistant Professor. He also worked as a researcher at the Photovoltaic Materials Unit, National Institute for Materials Science (NIMS), Tsukuba, Japan, before joining as a scientist at CSIR-IICT in 2011. He has published over 230 papers and reviews in peer-reviewed journals and patents and edited two books and is the author of one book chapter. BODIPY based dyes for mitochondrial tracking developed by Singh and colleagues have been licensed and commercialised by TCI (Japan). During his tenure at CSIR-IICT he has been a recipient of several prestigious awards like the CRSI-bronze medal (2024), NASI-young scientist platinum jubilee award (2012), and AVRA young scientist award (2015). Dr Singh is a Fellow of Telangana academy of sciences (2022) and Associate Fellow of Andhra Pradesh academy of sciences (2013) and Indian National Science Academy-INSA (2024). He has been awarded the Bhaskara Advanced Solar Energy (BASE) Fellowship by the Indo-U.S. Science and Technology Forum (IUSSTF) to work at the University of California, Santa Barbara. Dr S. P. Singh has made outstanding contributions in chemistry and chemical technologies, particularly materials and molecules for photonic devices as emerging renewable energy resources and development of functional π-conjugated dyes.

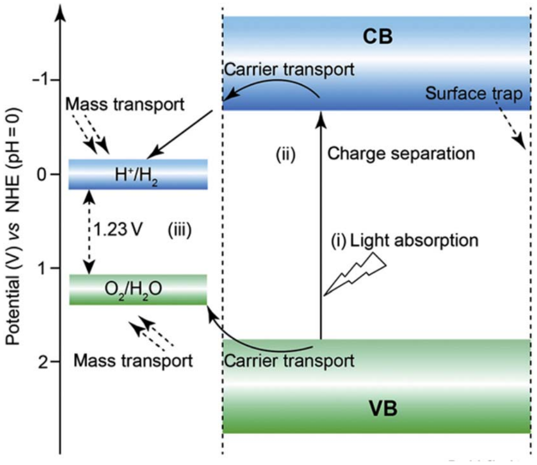

Fig. 1 Mechanism for photocatalytic hydrogen gas evolution. Reproduced with permission from ref. 29, Copyright © 2020, Elsevier.

on the photocatalyst surface. The effective separation of electrons and holes on the catalyst surface, and a decreased rate of charge recombination play very important roles in the photocatalysis process. The hydrogen evolution and oxygen evolution reaction involve the following reactions,

$$2H_2O + 4\,h^+ \rightarrow 4H^+ + O_2 \quad (1)$$

and

$$4H^+ + 4e^- \rightarrow 2H_2 \quad (2)$$

Theoretically, minimum photon energy required for an overall water splitting (OWS) reaction is 1.23 eV. For an effective photocatalysis reaction, the conduction band minimum of the photocatalyst should be more negative than the H^+/H_2 energy level, while the valence band maxima should be more positive than the O_2/H_2O energy level. Semiconductor metal oxides are found to have excellent photocatalytic activity for the hydrogen evolution reaction. Usually, metals with d^0 or d^{10} are active elements for photocatalysis and are introduced to construct the valence band, while the conduction band is formed from non-metal elements (O, S, and N).[16,30] Other than a catalyst, co-catalysts play a very important role in PHE. They lower the activation energy of the reaction by providing redox reaction sites. Noble metals are extensively used as co-catalysts for the PHE reaction; however, their scarcity limits their application for large-scale reactions.

Small molecules play a major role in green energy production due to their easy synthesis and purification process. Moreover, their energy level can be modulated by molecular engineering. A series of small molecules have been successfully demonstrated for various photonic devices such as dye-sensitized solar cells (DSSCs), organic solar cells, perovskite solar cells, organic light-emitting diodes, *etc.*[31–41] Recently small molecules have attracted great attention towards the production of hydrogen fuel through photocatalysis. The fundamental requirements for small molecules to be effective photocatalysts for the hydrogen evolution reaction are, (a) broad absorption of organic small molecules covering the UV-visible-NIR range, which can be achieved *via* reducing the band gap of the semiconductor by increasing the conjugation, functionalizations, planarization, *etc*. The lower band gap will maximise absorption of the solar spectrum and increase solar to hydrogen fuel conversion efficiency. (b) Appropriate positioning of the energy level with respect to the proton reduction energy level. (c) Optimum exciton separations play a very important role in photocatalysis. Therefore, factors such as the exciton diffusion length, hetero-junction assembly, use of co-catalysts and sacrificial reagents, size modulation of nano-aggregates, *etc.* contribute to efficient exciton dissociation and reduced charge recombination. (d) Metal photocatalysts benefit from fast charge transport resulting in a high photocatalytic rate. Therefore, the factors which increase the charge transport in small molecule semiconductors are effective overlap of pi orbitals, delocalization of pi-electron density through donor/acceptor interaction, strong intramolecular interactions, close packing, crystallinity, *etc.* which will significantly improve the photocatalytic rate. (e) Crystallinity or ordering in self-assembly increases the stacking interaction within molecules and contributes to the improvement in light absorption and charge transport properties.[42–45] Various classes of functional π-conjugated small molecules containing extended pi-conjugated chromophores, conjugated donor–acceptor units, and amphiphilic and charged functional groups are reported for the photocatalytic hydrogen evolution reaction, which are summarized below:

2.1 Conjugated donor–acceptor small molecules

Conjugated donor–acceptor molecules are aromatic conjugated moieties having two or more chromophores of opposite electron affinity connected by C–C bonds. They have recently been studied for the photocatalytic hydrogen evolution reaction due to their intrinsic characteristics of broad absorption, good quantum yield of emission, and efficient exciton separation. The complementary electron affinity of an electron-rich donor and electron-deficient acceptor makes the electron density concentrated towards the acceptor part of the molecule and facilitates exciton separation. Cloutet and co-workers reported donor–acceptor-donor conjugated trimer-type small molecules for the photocatalytic hydrogen evolution reaction (Fig. 2).[46] The photocatalytic efficiency was tuned by using carbazole (C), thiophene (T), and 3,4-ethylenedioxythiophene (E) as electron donors, and benzothiadiazole (B) and quinoxaline (Q) as acceptors. Solid-state absorption spectral analysis showed a broad absorption band for all six derivatives (CQC, CBC, TQT, TBT, EQE, and EBE) with EBE, EQE, and TBT showing more extended absorption in the visible range. TEM investigation of microaggregates, prepared by a reprecipitation method showed the crystalline nature of the aggregate, which is beneficial for long-range ordering and charge transport. The photocatalytic activity was checked for all trimers with triethanolamine (TEOA) as a sacrificial hole scavenger. The photocatalytic hydrogen

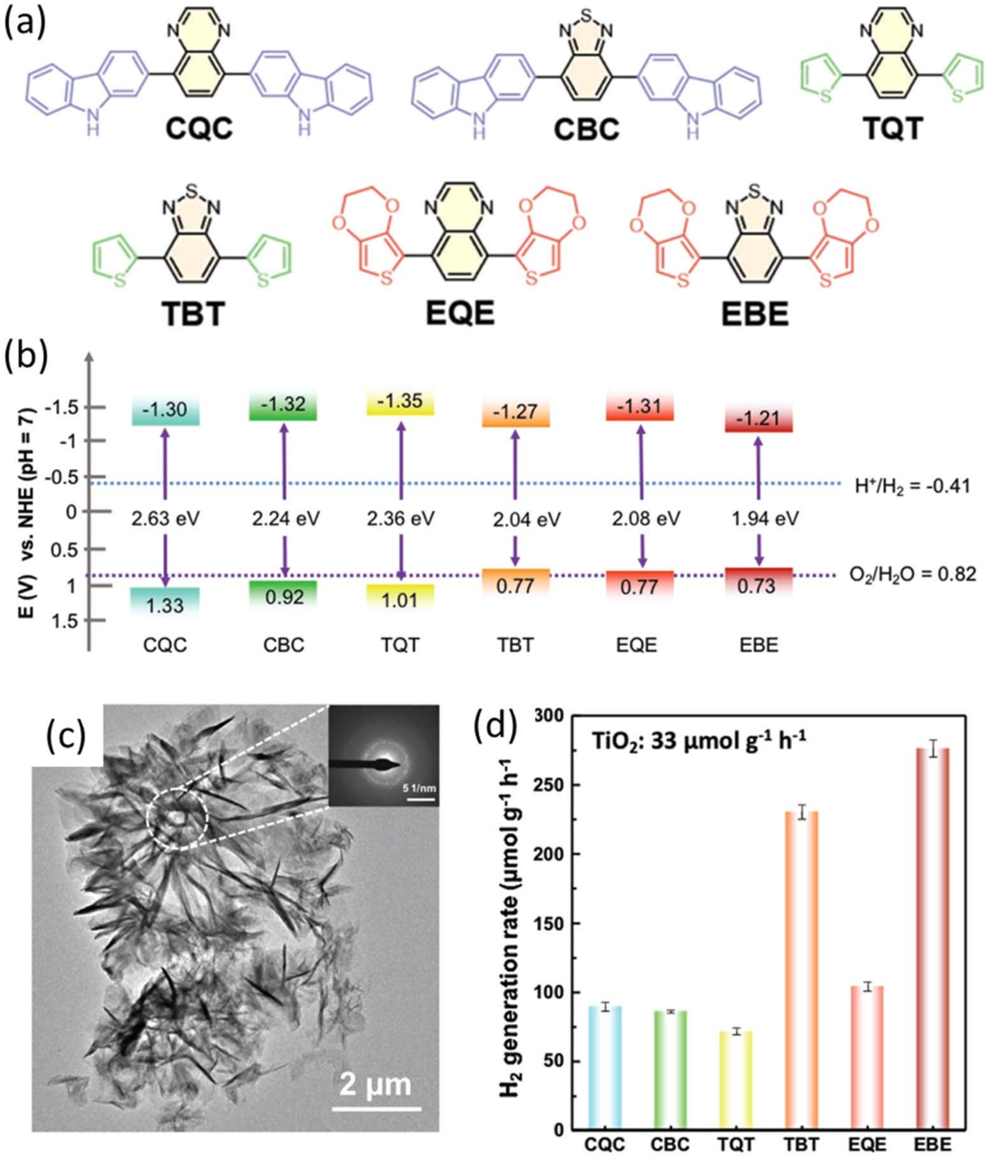

Fig. 2 (a) The chemical structure of trimer photocatalysts, (b) HOMO and LUMO energy levels experimentally determined for trimers, (c) TEM image of the microaggregate of an EBE trimer, and (d) normalized H_2 production of trimers under UV-vis light. Reproduced with permission from ref. 46, Copyright © 2023, John Wiley and Sons.

evolution activity of all trimers was observed to be higher than that of the TiO_2 semiconductor, which is due to a lower band gap within the 1.94–2.63 eV range compared to TiO_2 (3.2 eV) facilitating light harvesting capacity of the trimer; moreover, band positions are suitable for proton reduction. The highest photocatalytic activity was found for EBE with a HER of 275 μmol h^{-1} g^{-1} and 142 μmol h^{-1} g^{-1} under UV and visible light irradiation (Table 1). The addition of a Pt co-catalyst was found to reduce the photocatalytic performance of EBE; therefore, co-catalyst addition was not required for photocatalytic purposes. Enhanced photocatalytic H_2 evolution activity of the EBE-TiO_2 heterojunction composite was observed due to the formation of a p–n heterojunction, which can be an advantageous way to increase the photocatalytic hydrogen evolution activity for small molecule photocatalysts.

Zhang and co-workers reported conjugated donor–acceptor–donor type trimer molecules for photocatalytic hydrogen evolution (Fig. 3).[47] They have investigated the effect of single-atom substitution on the band gap, HOMO and LUMO energy levels and photocatalytic hydrogen evolution activity of the small molecules. The molecules were designed by attaching peripheral pyrazole units with different centre aromatic cores by the substitution of a single atom (O, S, or Se), *i.e.*, M1–M4, and by controlling the number of N atoms by replacing the peripheral donor with benzene, pyridine or pyrazole *i.e.*, CM1, CM2, and M1. They observed good photocatalytic performance for molecules with a less deep LUMO level and wide absorption band. Also, the increase in nitrogen atoms increases the dispersibility in water by H-bonding interaction; moreover, nitrogen atoms act as active sites for the photocatalytic reaction.

Table 1 Summary of small molecules discussed for the photocatalytic hydrogen evolution reaction

Sr. no.	Small molecules	Type	Light source	Sacrificial reagent	Co-catalyst	HER	Ref
1	EBE	Donor–acceptor–donor trimer	UV	TEOA	—	275 µmol h^{-1} g^{-1}	46
2	EBE	Donor–acceptor–donor trimer	Vis	TEOA	—	142 µmol h^{-1} g^{-1}	46
3	M1	Conjugated trimer	Visible light ($\lambda \geq 420$ nm)	TEOA	Pt	4 µmol h^{-1} for 50 mg of M1	47
4	CzPn	Donor–acceptor	Visible light ($\lambda \geq 420$ nm)	TEOA	Pt	91.8 µmol h^{-1} (20 mg of CzPn)	48
5	PCPyBDT	Donor–acceptor	300 W Xe-lamp ($\lambda > 420$ nm)	TEOA	H_2PtCl_6	8143 µmol g^{-1} h^{-1} (ground state) 3943 mmol g^{-1} h^{-1} (without grinding)	49
6	F1	Organic photovoltaics	AM 1.5G (100 mW cm^{-2})	Ascorbic acid	Pt	152.60 mmol h^{-1} g^{-1}	50
7	Y6CO	Organic photovoltaics	AM 1.5G light, 100 mW cm^{-2}	Ascorbic acid	Pt	230.98 mmol h^{-1} g^{-1}	51
8	PM6:Y6CO	Organic photovoltaics	AM 1.5G light, 100 mW cm^{-2}	Ascorbic acid	Pt	323.22 mmol $h^{-\ 1}$ g^{-1}	51
9	Chiral Y6CO	Organic photovoltaics	AM 1.5G, 100 mW cm^{-2}, simulated solar light	Ascorbic acid	Pt	205 (Y6-S) and 217 (Y6-R) mmol h^{-1} g^{-1}	52
10	rubrene/ZnP-NS/methyl viologen	Porphyrin derivative	300 W Xe lamp	TEOA	$H_2PtCl_6 \cdot 6H_2O$	9.3 mmol g^{-1} h^{-1}	53
11	(ProFN) + 0.5 mM sodium chloride	Water-soluble porphyrin derivative	Simulated solar power (AM 1.5G, 100 mW cm^{-2})	TEOA	Pt	10.9 mmol h^{-1} g^{-1}	54
12	Amphiphilic perylene monoamide	Perylene derivative	21 V, 150 W EKE halogen bulb	Ascorbic acid	Nickel catalyst ([Ni(P2 PhN2 Ph)2](BF4)2)	19 h^{-1}	55
13	NH_2-CA CH_3-CA	Perylene derivative		Ascorbic acid	Mo_3S_{13}	94 ± 14 µmol g^{-1} h^{-1} 160 ± 21 µmol g^{-1} h^{-1}	56
14	Perylene tetracarboxylic acid	Perylene derivative	Visible light	Ascorbic acid	Pt	118.9 mmol g^{-1} h^{-1}	57
15	PPT-g-CN and PTP-g-CN	Organic heterojunction nanoparticles	Visible light ($\lambda > 420$ nm)	TEOA	H_2PtCl_6	3.41 mmol h^{-1} g^{-1} 7.71 mmol h^{-1} g^{-1}	58
16	POZ-M donor and ITC acceptor	Heterojunction nanoparticles	LED 50 mW cm^{-2} in 420–750 nm	Ascorbic acid	Pt	63 mmol g^{-1} h^{-1}	59

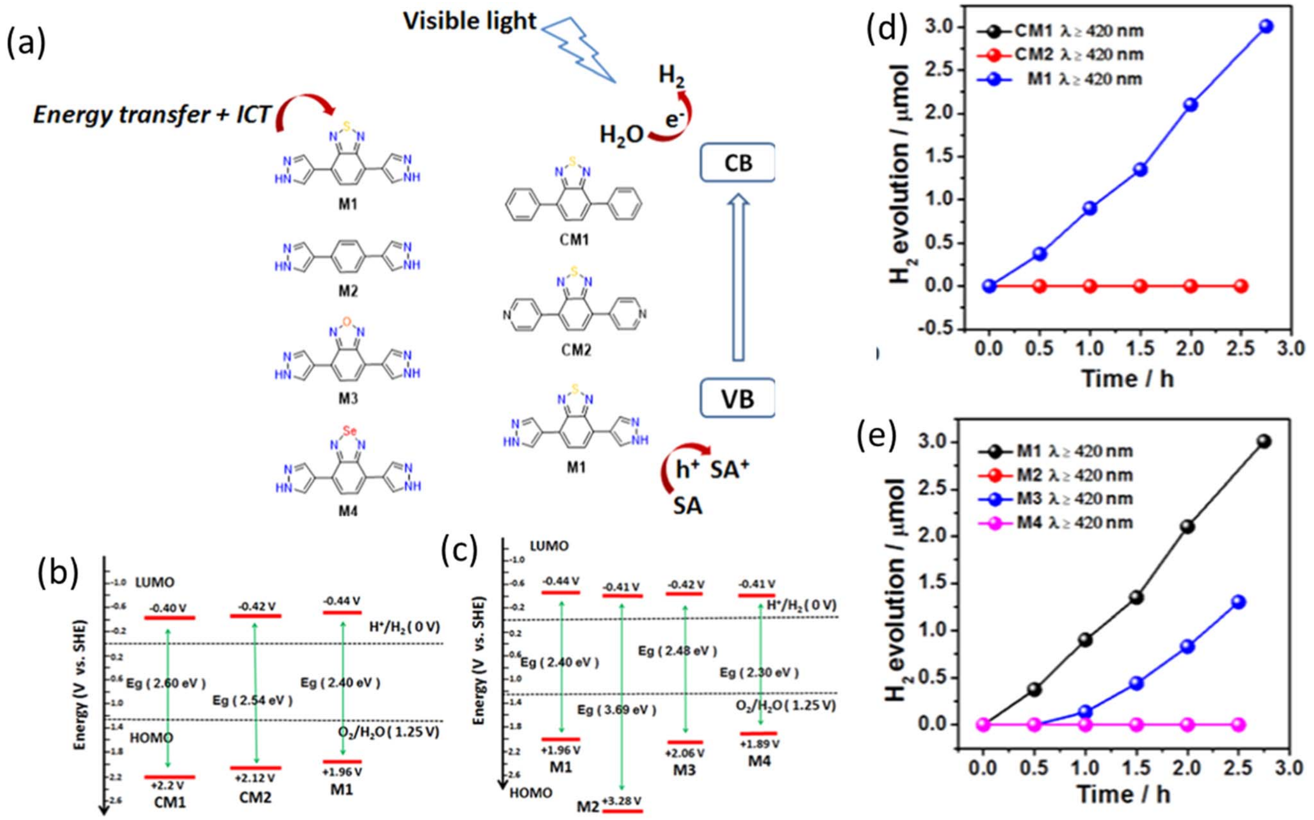

Fig. 3 (a) Chemical structure of conjugate trimers. (b and c) Calculated HOMO and LUMO band positions of CM1, CM2, M1, and M1–M4. (d) Temporal photocatalytic H_2 evolution of CM1, CM2, and M1 under visible light illumination ($\lambda \geq 420$ nm) and (e) temporal photocatalytic H_2 evolution of M1–M4 under visible light illumination ($\lambda \geq 420$ nm). Reproduced with permission from ref. 47, Copyright © 2020, American Chemical Society.

The optical band gaps for CM1, CM2 and M1 were found to be 2.60, 2.54, and 2.40 eV, respectively and 2.40, 3.69, 2.48, and 2.30 eV for M1–M4, respectively. The HOMO and LUMO energy level calculation showed that the LUMO of CM1 and CM2 is not negative enough for proton reduction. Similar observations were made for M1–M4 systems, where heavy atom substitution significantly impacts the optical band gap. When photocatalytic activity was studied with 10% TEOA as the sacrificial reagent and 1 wt% Pt as the co-catalyst, the highest photocatalytic efficiency was found for M1 with a HER of 4 μmol h^{-1} for 50 mg of the catalyst with an order of M1 > M3 > M4 > M2. The author concluded that the presence of the highest number of nitrogen atoms, a suitable band gap, and an appropriate position of the LUMO energy level of M1 promotes efficient photocatalytic HER.

Li and coworkers recently reported donor–acceptor-donor pi-conjugated trimers with methyl substitution at different positions of the terminal thiophene donor units. They found that the 3-methyl substitution on terminal thiophene was showing excellent photocatalytic hydrogen evolution activity attributed to long-range ordering and a shorter distance for charge carrier separation.[60]

Zhang *et al.* investigated the cyanocarbazole derivative CzPn in the supramolecular state and polymeric state for photocatalytic hydrogen gas evolution.[48] The supramolecules of CzPn showed crystalline plate-like morphology and the CzPn polymer showed rod-like granular structures (Fig. 4). UV-vis diffuse-reflectance spectral analysis showed that both the CzPn supramolecule and polymer have strong absorption bands in the visible region, with the polymer having a more expanded absorption range due to the greater extent of conjugation by covalent bonding. The band gap of the supramolecule and polymer calculated from the Tauc plot were 2.37 and 2.22 eV, respectively. The photocatalytic hydrogen gas evolution activity of the CzPn supramolecule with 1% Pt as the co-catalyst and triethanolamine as a sacrificial agent under visible light irradiation was found to be 91.8 μmol h^{-1} ($\lambda > 420$ nm), which is 2.7 and 20.9 times higher than that with L-ascorbic acid and methanol as the sacrificial agent, respectively. The PHE activity of the polymer was found to be half that of the CzPn supramolecule, even though the Brunauer–Emmett–Teller BET absorption area and light absorption are significantly broader. The higher catalytic activity of the supramolecule is due to the higher crystallinity favouring strong donor–acceptor interaction and better charge separation. The HOMO and LUMO of the CzPn molecule were found to be well separated with a LUMO value −0.92 *vs.* NHE and HOMO value 1.45 *vs.* the normal hydrogen electrode (NHE), which is favourable for generation of H_2 gas from H_2O using a Pt catalyst. The apparent quantum efficiency (AQE) of the CzPn supramolecule was found to be

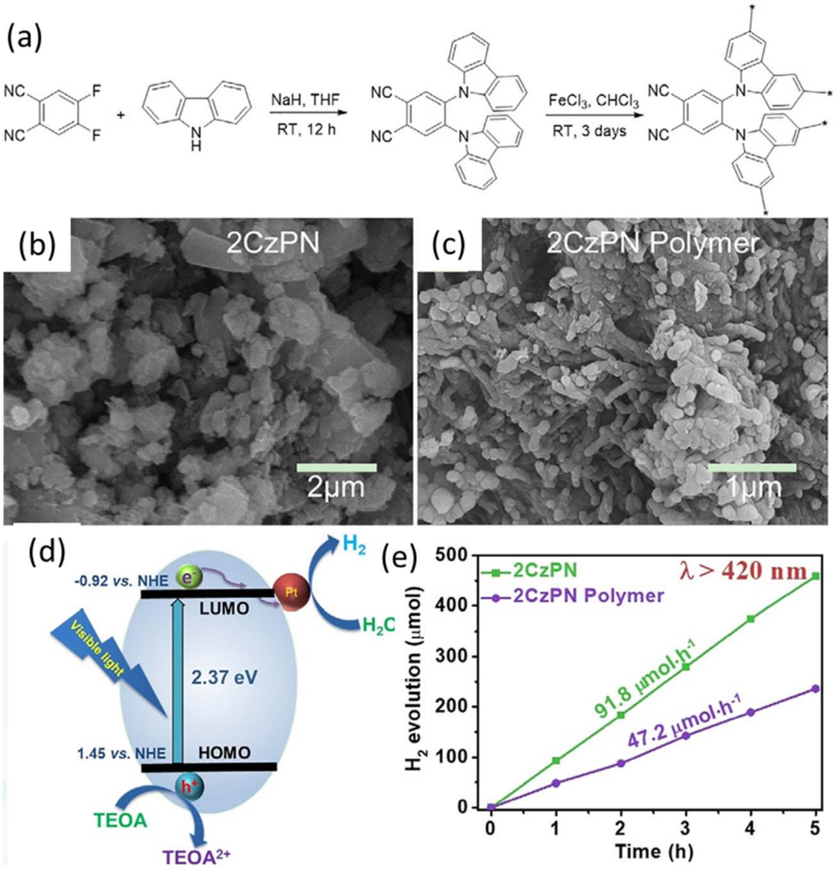

Fig. 4 (a) Synthetic scheme for 2CzPN supramolecule and polymer preparation, (b) SEM image of the 2CzPN supramolecule, (c) SEM image of the 2CzPN polymer, (d) schematic diagram for photocatalytic hydrogen production by the 2CzPN supramolecule, and (e) the comparison of photocatalytic hydrogen production by the 2CzPN supramolecule and polymer. Reproduced with permission from ref. 48, Copyright © 2019, John Wiley and Sons.

7.5%, 6.1%, and 0.8% at 420 nm; at 475 nm, and at 550 nm, respectively.

The effect of crystallinity on the photocatalytic hydrogen evolution reaction is demonstrated by Wan *et al.* They designed crystalline micro/nanosheets of a conjugated donor–acceptor molecule containing benzo[1,2-*b*:5,4-*b*′]dithiophene (BDT) as the electron donating unit and cyano-functionalized pyridine as the electron withdrawing unit for photocatalytic hydrogen evolution. The molecule crystallized into a sheet shape crystal with a long-range ordered stacking arrangement (Fig. 5).[49] The highly compact arrangement of the molecules favours efficient intra- and intermolecular donor–acceptor interaction, which facilitates charge migration from the bulk phase to the surface where the electron is captured by a co-catalyst and hole by a sacrificial reagent suppressing exciton recombination, and charge transport mobility was reported to be 0.25 cm^2 V^{-1} s^{-1}. The broader bandwidth and red shift in UV-vis absorption and photoluminescence spectra were observed for the crystal state compared to diluted solution which indicates strong absorption properties of the crystal. The photocatalytic hydrogen evolution experiment in the presence of triethanolamine (TEOA) and hexachloroplatinic acid(H_2PtCl_6) as the hole scavenger and co-catalyst, respectively showed that the HER was highly efficient with a rate of 8143 μmol g^{-1} h^{-1} in the ground state and 3943 mmol g^{-1} h^{-1} without grinding. Therefore, as a rugged surface decreased transparency, an enhanced hydrogen evolution rate was observed. The AQE was calculated to be 3.9% and 3.5% at 405 nm and at 420 nm, respectively.

2.2 Organic photovoltaic small molecules

Organic photovoltaic molecules possess broad absorption in the visible range and showed promising solar energy to electricity conversion efficiency (18–20%),[61–63] Recently, they have attracted increased attention as photocatalysts for hydrogen fuel production. A shorter exciton diffusion length (5–10 nm) and high exciton binding energy in organic semiconductors severely limit their photocatalytic performance. Therefore, there is a requirement to increase the exciton diffusion length. Lin and co-workers reported a photovoltaic organic photocatalyst with nitrogen heterocyclic electron-donating units at both ends connected with the centre benzene core (Fig. 6).[50] The F1 film was found to have absorption extended till 901 nm with a higher molar extinction coefficient. The molecule was observed to have high quantum yield (9.3%) in emission. Grazing incidence wide-angle X-ray scattering (GIWAXS) showed a high crystalline coherence length (CCL) both in the in plane and out of plane

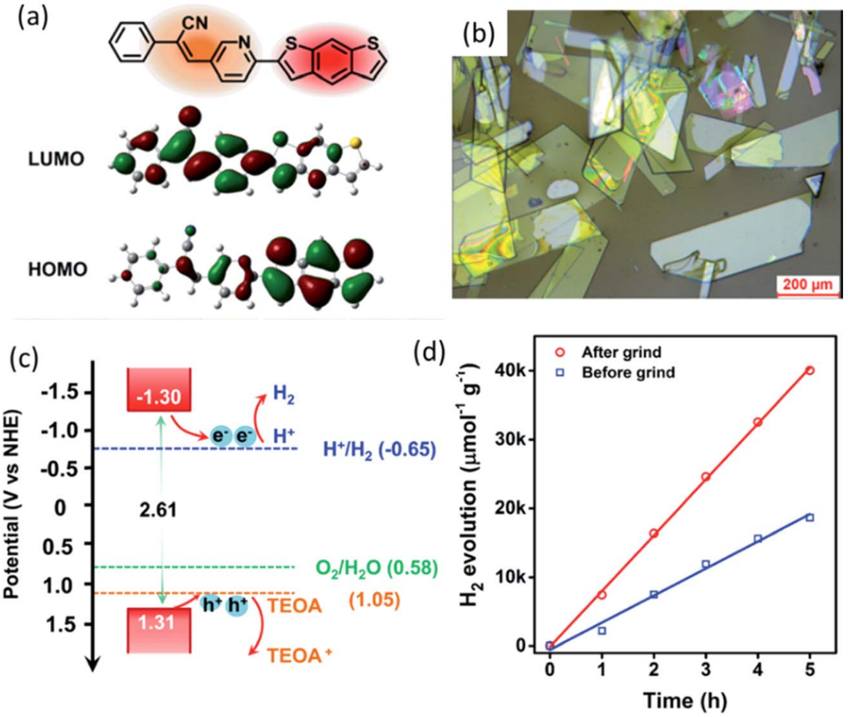

Fig. 5 (a) The chemical structure and HOMO/LUMO distribution of PCPyBDT, (b) the microscope images of a sheet like single crystal under normal light, (c) the band gap alignment calculated by the CV method, and (d) HER activity study with PCPyBDT sheets before and after grinding. Reproduced with permission from ref. 49, Copyright © 2021, Royal Society of Chemistry.

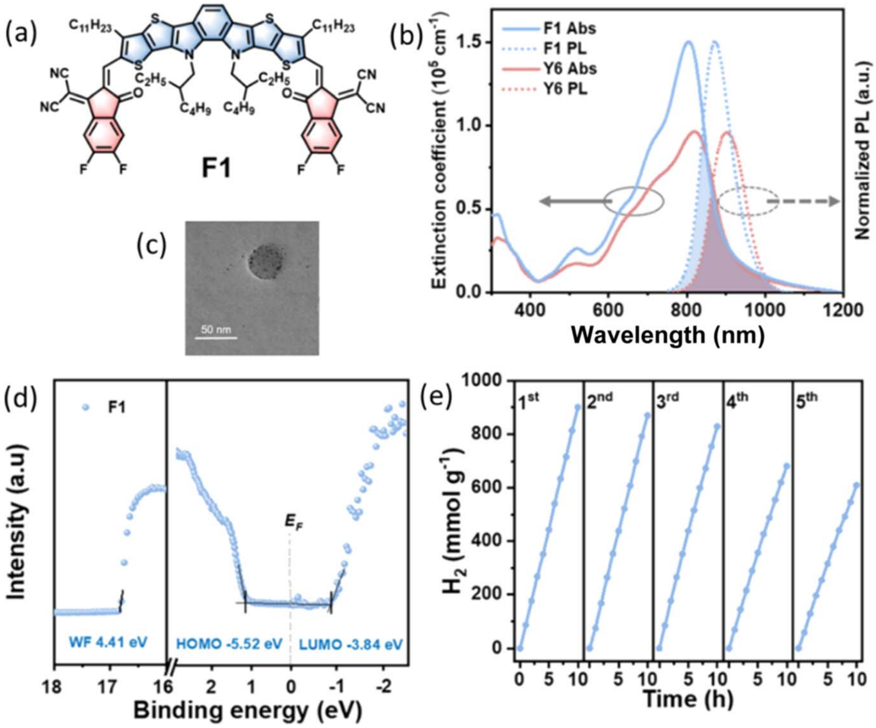

Fig. 6 (a) Chemical structure of the photovoltaic organic photocatalyst (F1) and (b) absorption coefficient and normalized PL of the F1 film and Y6 film. (c) Cryo-TEM image of Pt cocatalyst deposition of F1 NPs. (d) UPS and LEIPS spectra of F1, with respect to the Fermi energy level (EF) at 0 eV (work function (WF) values are labelled). (e) F1 NPs (6.67 μg mL^{-1}) under AM 1.5G (100 mW cm^{-2}) investigated for recycling experiments of hydrogen evolution. Reproduced with permission from ref. 50, Copyright © 2022, American Chemical Society.

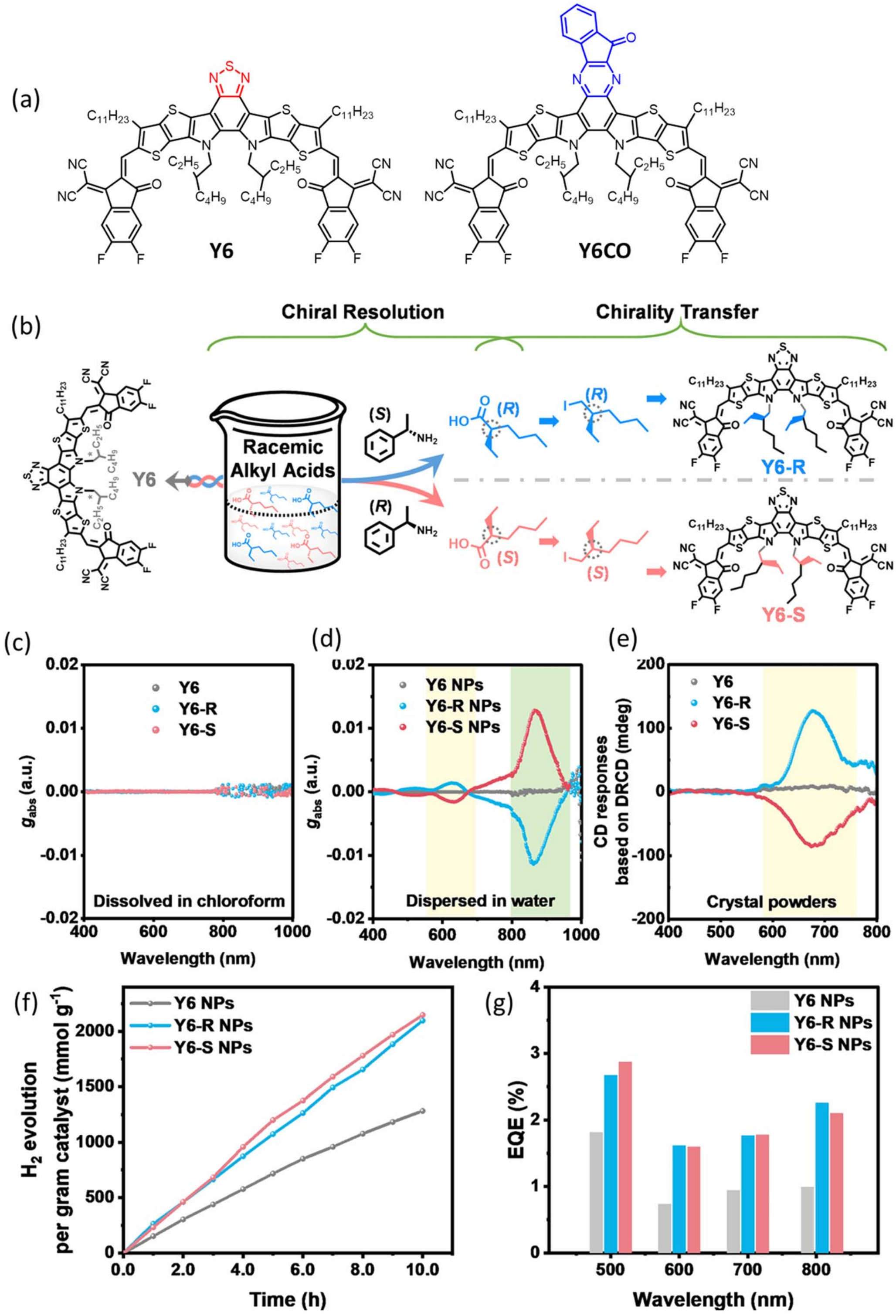

Fig. 7 (a and b) Chemical structures of Y6, Y6CO, Y6-S, and Y6-R and (c) the CD spectra recorded for Y6, Y6-R, and Y6-S in chloroform solution. The g_{abs} is the dissymmetry factor. (d) The CD spectra recorded for Y6, Y6-R, and Y6-S NPs dispersed in water. (e) The diffuse reflection circular dichroism (DRCD) spectra were recorded for single crystal powders of Y6, Y6-R, and Y6-S. (f) Hydrogen evolution per gram catalyst *vs.* illumination time of Y6, Y6-R, and Y6-S NPs under AM 1.5G, 100 mW cm^{-2} simulated solar light. (g) EQE of Y6, Y6-R, and Y6-S NPs at 500, 600, 700, and 808 nm. Reproduced with permission from ref. 52, Copyright © 2023, John Wiley and Sons.

directions. Therefore, the F1 film has fewer grain boundaries, resulting in higher QY, contributing to an increased exciton diffusion length (L_D) (20 nm),[64,65] which led to efficient charge separation for the hydrogen evolution reaction. When hydrogen evolution performance was evaluated for F1 nanoparticles with a 0.4 wt% sodium 2-(3-thienyl) ethyloxybutylsulfonate (TEBS) surfactant, 33 wt% Pt as the co-catalyst and ascorbic acid as the sacrificial reagent, the highest average HER maximum was found to be 152.60 mmol h^{-1} g^{-1} for (15.63 μg mL^{-1}) for 10 h under AM 1.5G (100 mW cm^{-2}).

Cryo-transmission electron microscopy showed the NPs with a 44.2 ± 14.8 nm diameter and the recyclability study showed good stability of NPs with HER rates of 77% and 68% for the first cycle. The photocatalytic HER of F1 NPs was one of the highest reported among organic photocatalysts and much better than that of many inorganic photocatalysts.

Lin and co-workers designed an organic photovoltaic molecule Y6CO (Fig. 7) with a carbonyl group for attaching to Pt by σ–π coordination, which lowers the energy as well as stabilizes the Pt in the metallic state.[51] The photocatalytic hydrogen evolution investigation showed an enhanced HER of 230.98 mmol h^{-1} g^{-1} and 323.22 mmol h^{-1} g^{-1} for Y6CO and PM6/Y6CO (PM6 acts as a polymer donor) heterojunction nanoparticles under simulated solar light which is four times higher than that of Y6 nanoparticles without any coordination site, and external quantum efficiency for PM6/Y6CO heterojunction nanoparticles was found to be 10% under visible and NIR light. Therefore, σ–π anchoring is demonstrated as a useful strategy for the integration and stabilization of metallic co-catalysts for the photocatalytic HER, which can be extended to other photocatalyzed reactions. The same group reported chiral organic semiconductors having chiral alkyl chains for the photocatalytic HER. Upon the introduction of the chiral alkyl chain on the conjugated main chain of chiral nanoparticles, it exhibits reduced charge recombination due to chirality-induced spin polarization (Fig. 7).[52] As a result, the chiral Y6-S and Y6-R analogues exhibit 60–70% higher photocatalytic activity than achiral Y6. The circular dichroism (CD) spectral analysis showed the silent CD response in chloroform solution of both Y6-S and Y6-R derivatives, whereas a pronounced CD signal was observed from the aggregated state of the NP dispersion in water, with a positive CD response from Y6-R and negative CD response from Y6-S, respectively.

Employing the photoelectrochemical method, the effect of chirality-induced spin polarization of Y6-R and Y6-S NPs on the amount of available delocalized charge was investigated on a fluorine doped tin oxide (FTO) electrode, which exhibits

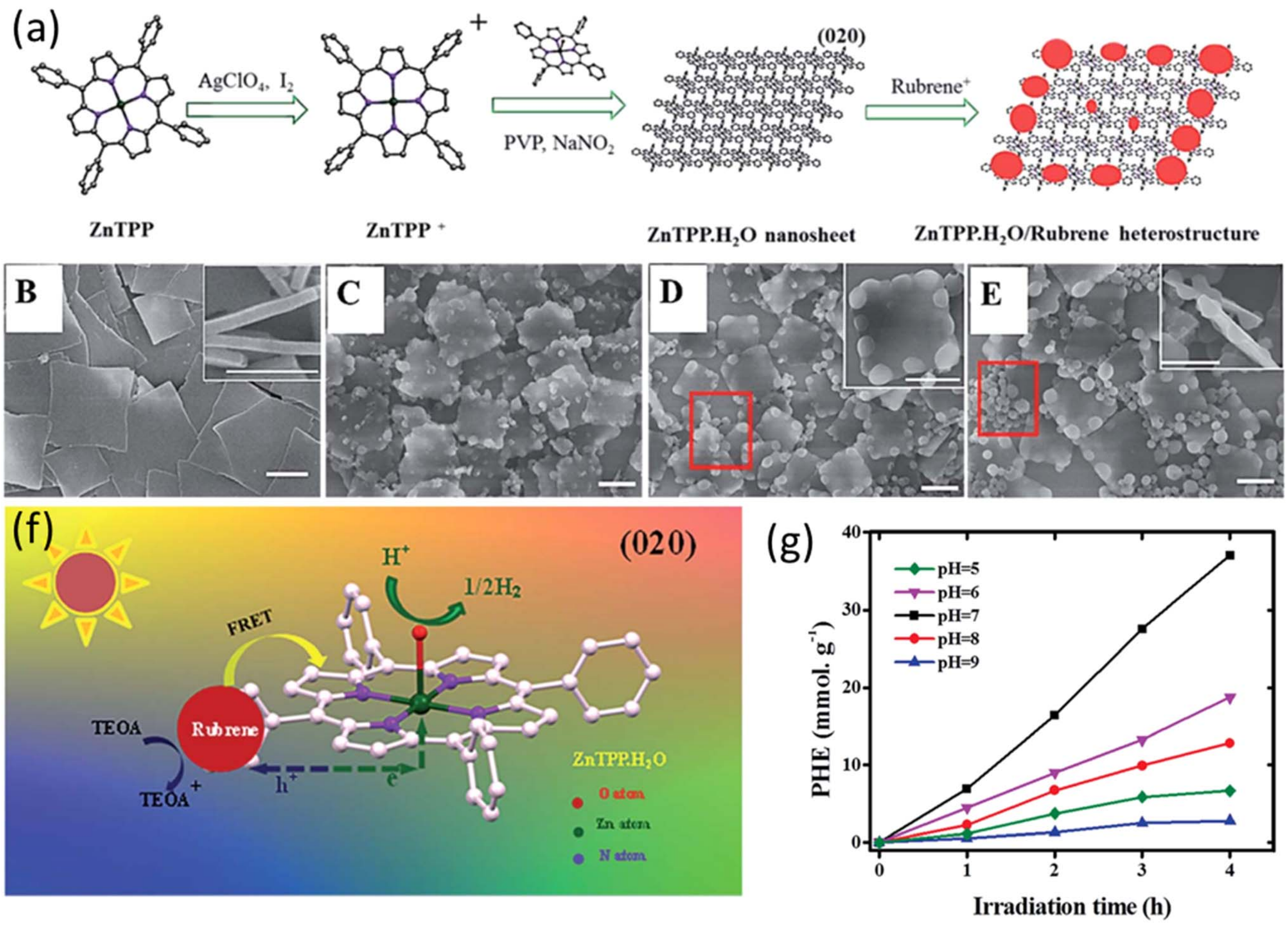

Fig. 8 (a) Schematic representation of the preparation of the ZnP NS and rubrene-ZnP NS heterostructure in the aqueous solution; SEM images of (b) only ZnP NS and, rubrene-ZnP NS heterostructure with (c) 1 : 6, (d) 1 : 3 and (e) 2 : 3 molar ratios of rubrene: ZnP, and (f) schematic representation of consecutive photoexcited electron transfer, FRET, and photo hydrogen evolution under light irradiation over the rubrene-ZnP NS photocatalyst. (g) PHE of rubrene/ZnP-NS (3 : 1) over time at different pH with MV, TEOA, and 3.8 wt% Pt present in aqueous system. Reproduced with permission from ref. 53, Copyright © 2016, Royal Society of Chemistry.

higher photocurrent density than achiral Y6 NPs. In a photocatalytic activity study with Pt as the co-catalyst, higher hydrogen evolution was observed for chiral NPs than achiral ones under the same experimental conditions, which indicates the significant impact of chirality on photocatalytic activity. With 16% Pt loading, an optimum nanoparticle concentration of 3.33 μg mL^{-1} and ascorbic acid as the sacrificial agent, Y6-S and Y6-R showed a hydrogen evolution rate (HER) of 205 and 217 mmol h^{-1} g^{-1}, which is higher than that for Y6 NPs with a hydrogen evolution rate of 129 mmol h^{-1} g^{-1} under AM 1.5G, 100 mW cm^{-2} simulated solar light for 10 h. Under the optimized conditions when the concentration is higher than 26.67 μg mL^{-1} for Y6-S and Y6-R NPs, the external quantum efficiency (EQE) was found to be 1.5–2 times higher than that of Y6 NPs with 2.7%, 1.6%, 1.7%, and 2.1% at the wavelengths of 500, 600, 700, and 808 nm. Therefore, a higher HER and EQE signify the significant impact of spin polarization on charge-carrier separation, although the similar HER and photoelectrochemical measurement exclude the possibility of chirality selective catalysis. On blending Y6-R/S NPs with 20% polymer a reduction in CD signal and photocatalytic activity was observed, which supports that chirality-induced spin polarization reduced the charge-carrier recombination and improved the photocatalytic hydrogen evolution rate.

2.3 Porphyrin based small molecules

Porphyrin with a large conjugated macrocyclic core shows good light harvesting properties and excellent electron delocalization. It is possible to modulate the band structure required for efficient photocatalysis. Yao and coworkers reported a zinc

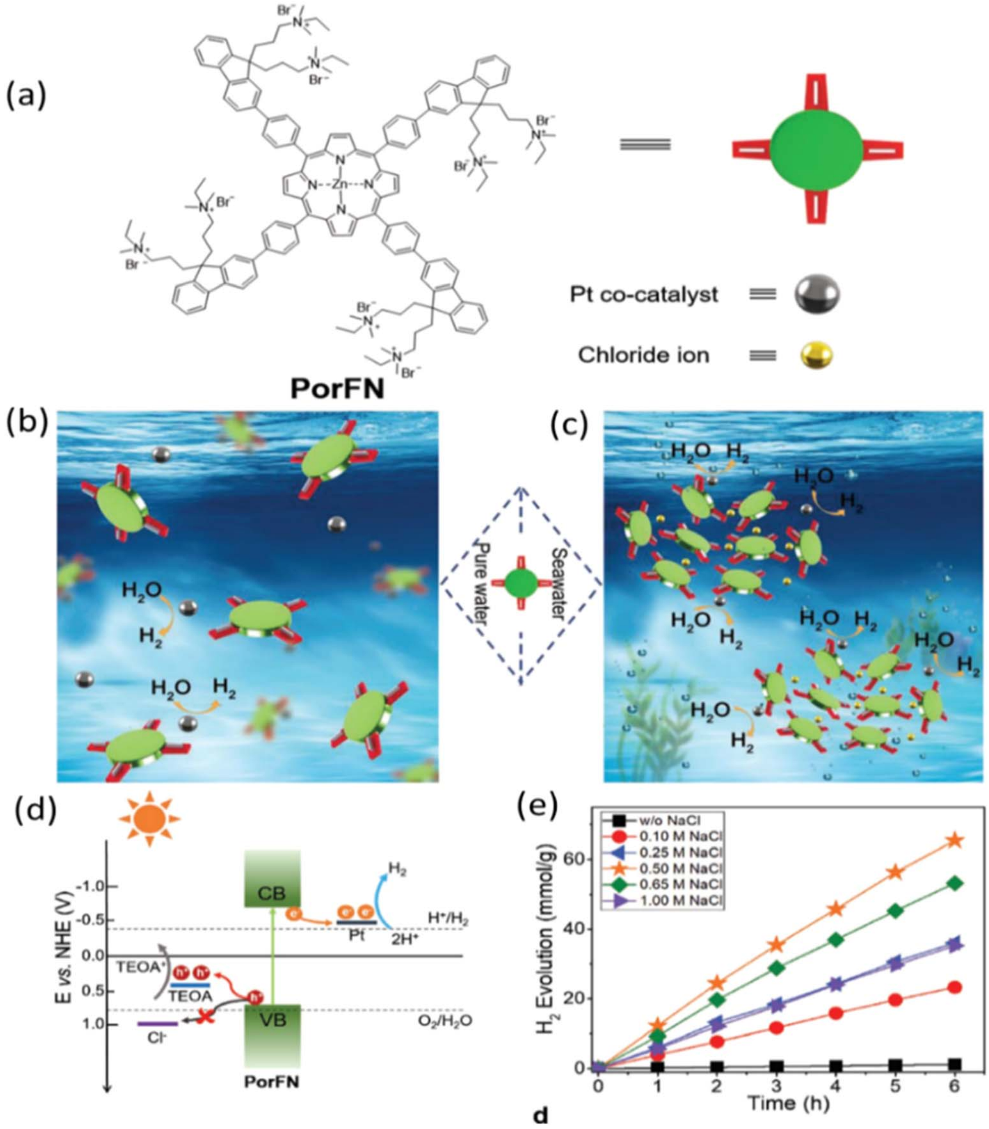

Fig. 9 (a) The chemical structure of Pro-FN and schematic presentation of photocatalytic hydrogen evolution by Por-FN in the (b) monomeric and (c) self-assembled state in salt water. (d) Energy level diagram of PorFN, TEOA, and chlorine ions at pH = 7. (e) Photocatalytic hydrogen evolution study for PorFN in the presence of TEOA as the sacrificial reagent and Pt as the cocatalyst with simulated solar light (AM 1.5G, 100 mW cm^{-2}). Reproduced with permission from ref. 54, Copyright © 2019, John Wiley and Sons.

porphyrin (ZnP) based derivative as a hydrated supramolecular nanostructure for the PHE reaction.[53] The author reports synthesis of a ZnP nanostructure by the liquid phase chemical reaction method with the formation of square nanoflakes which have an edge length of 900 nm and a thickness of <100 nm (Fig. 8). The PHE reaction was performed with ZnP as the photocatalyst and TEOA as a sacrificial electron donor. The PHE rate was observed to be 0.16 mmol g^{-1} h^{-1}. When ZnP as a photocatalyst was combined with rubrene as the photosensitizer in a 1 : 3 ratio, the PHE efficiency of the rubrene-ZnP heterostructure was improved with a PHE rate of 0.56 mmol g^{-1} h^{-1}. The formation of the rubrene/ZnP-NS heterostructure in the aqueous solution facilitates the FRET from rubrene to ZnP. As a result, light absorption capability of ZnP increases and the recombination of photoinduced electrons and holes get reduced. Further use of methyl viologen (MV) and $H_2PtCl_6 \cdot 6H_2O$ increased the PHE efficiency to 9.3 mmol g^{-1} h^{-1} at pH 7. MV functions as an electron relay for electron transfer from the photosensitizer rubrene to the Pt center, while Pt acts as a co-catalyst in the composite.

The water solubility and dispersibility of organic small molecules can be easily modulated by the introduction of charged and polar functional groups, unlike organic polymers. Cao and co-workers reported water-soluble positively charged porphyrin derivatives for the photocatalytic hydrogen evolution reaction (Fig. 9).[54] The porphyrin derivative (ProFN) contains four alkyl ammonium group functionalized cationic fluorene units connected to the *meso*-position of the porphyrin core *via* a phenyl bridge leading to enhanced light absorption and electron donating ability. The polycationic porphyrin derivative stays in the monomeric state in water with a particle size of 1.5 nm. Due to the limited interface contact area in the molecular state, the loading of the co-catalyst will be hindered. Therefore, self-assembly was induced by addition of chloride ions. With the addition of increasing concentration of sodium chloride (NaCl) *i.e.*, 0.1, 0.25, 0.5, 0.65, and 1.0 M, nano-aggregate formation was observed and particle size increases with sizes of 11.7, 91.3, 1281, 1718, and 3091 nm, respectively. Therefore, with increasing NaCl concentrations, larger aggregate formation was observed. The LUMO energy level (−0.74 eV) for proFN was found to be appropriate for the HER when

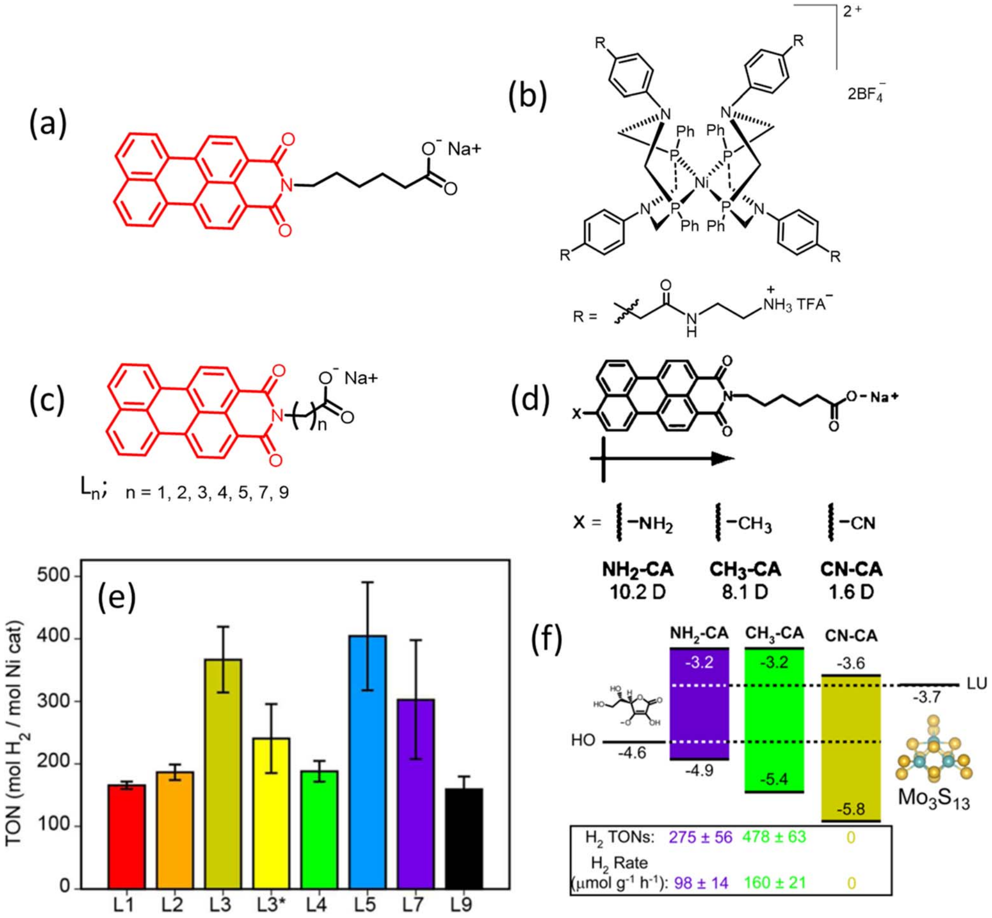

Fig. 10 (a) Chemical structure of amphiphilic perylene carboxylic acid derivative, (b) the chemical structure of the Ni catalyst, (c) chemical structure of perylene amphiphiles with different methylene linker lengths, (d) the chemical structures of perylene amphiphiles with electron-donating and withdrawing groups, and (e) the comparative representation of the TON for photocatalytic hydrogen evolution by different perylene amphiphiles. (f) Energy level diagram for perylene amphiphiles with oxidation potentials of ascorbate and a reduction potential of Mo_3S_{13}. Reproduced with permission from ref. 56, Copyright © 2018, American Chemical Society.

compared with NHE. The photocatalytic HER was performed employing PorFN along with TEOA as sacrificial hole scavengers and photo-deposited Pt nanoparticles as co-catalysts under irradiation of simulated solar power (AM 1.5G, 100 mW cm^{-2}).

It was observed that the photocatalytic hydrogen gas evolution rate increased drastically from 0.2 mmol h^{-1} g^{-1} for only monomeric pristine PorFN solution to 10.9 mmol h^{-1} g^{-1} with the addition of 0.5 mM sodium chloride. When the HER was carried out with simulated seawater, a similar HER (10.8 mmol h^{-1} g^{-1}) was observed. HER investigation with increasing intensity of simulated solar irradiation also showed increased HER with a rate of 8 mmol h^{-1} g^{-1} at an irradiation intensity of40 mW cm^{-2}, resembling morning sunlight or a cloudy day.

In a study from Wang's research group, they demonstrated metal-free porphyrin as a photocatalyst for both H_2 and O_2 evolution reactions under visible light irradiation without the use of a co-catalyst.[66] Araujo and co-workers designed a series of meso-substituted porphyrin derivatives containing donor–acceptor components for the hydrogen evolution reaction.[67] They have investigated the effect of chain length, atomic substitution of sulfur by selenium in the acceptor part, and extension of the thiophene donor unit on the photocatalytic hydrogen evolution reaction.

2.4 Perylene based small molecules

Stupp and coworkers explored perylene chromophores containing supramolecular self-assembly for light harvesting and solar-to-fuel conversion applications. In one of their seminal studies, they reported the amphiphilic perylene monoamide (PMI) derivative containing sodium hexanoate functionalized perylene anhydride as a self-assembled hydrogel scaffold for the catalytic hydrogen evolution reaction (Fig. 10a).[55] The use of hydrogel based soft materials has several advantages compared to photocatalysis in a solvent medium, *e.g.* the use of a large volume of solvent can be avoided, co-catalyst can be integrated into the gel fiber and device fabrication can be performed. The PMI amphiphilic derivative undergoes self-assembly with the formation of ribbon-like nanostructures which are approximately 40 ± 7 nm wide and several microns long. Furthermore, the addition of salt poly(diallyldimethylammonium) chloride (PDDA) (300 mM), $CaCl_2$ (150 mM) or NaCl (300 mM) for chromophore amphiphile (CA) assembly led to the formation of an irreversible gel. When the photocatalysis was performed with the overnight aged gel suspended in a solution containing a nickel catalyst ($[Ni(P_2\ PhN_2\ Ph)_2](BF_4)_2$) (Fig. 10b)[68] with ascorbic acid at pH 4, the hydrogen production turnover frequency (TOF) and turnover number (TON) were found to be 19 h^{-1} and 340 ± 50 in 150 hours, respectively. Similar photocatalytic activity was not observed for the solid precipitate of protonated CA. Therefore, the porous structure of the gel allows the diffusion of the Ni catalyst and ascorbic acid for efficient photocatalysis. The author performed photocatalytic hydrogen production with the hydrogel on glass, which showed a similar photocatalytic rate, although the rate diminishes with dried gel immersion in catalyst/ascorbic acid solution. This is the first report of the use of a small organic molecule-based hydrogel scaffold for photocatalytic hydrogen evolution.

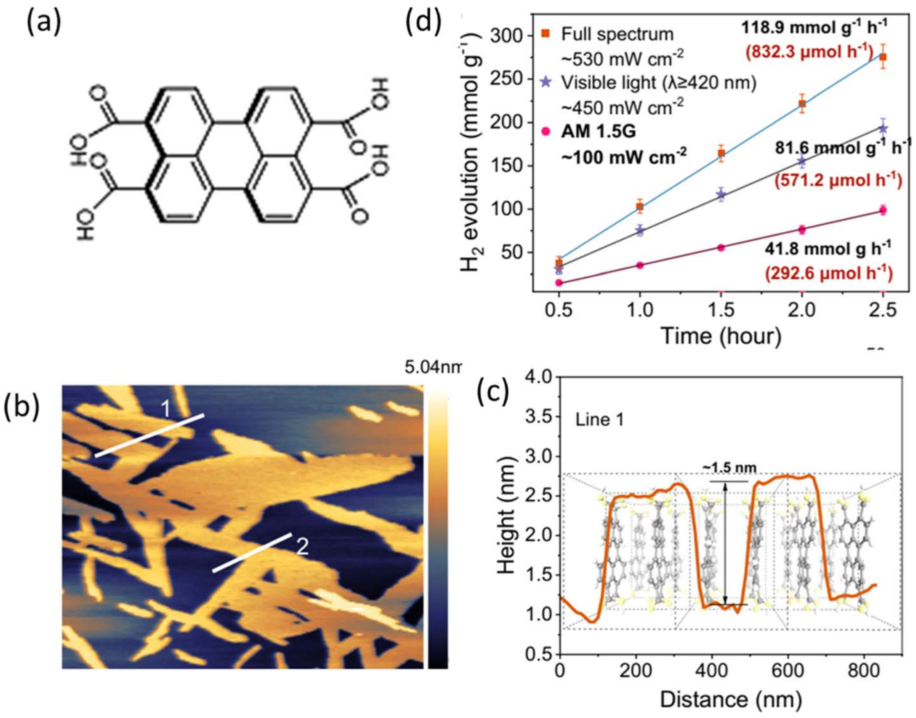

Fig. 11 (a) Chemical structure of perylene tetracarboxylic acid, (b) AFM images of PTA nanosheets, (c) the height profile and simulated structure comparison, and (d) the photocatalytic HER of PTA nanosheets under different irradiation conditions of the full spectrum (λ ≥ 300 nm), visible light (λ ≥ 420 nm) and AM 1.5G, (~100 mW cm^{-2}). Reproduced with permission from ref. 57, Copyright © 2022, Springer Nature.

The author further investigated the photocatalytic hydrogen evolution by using an amphiphilic perylene alkyl carboxylic acid self-assembled hydrogel with variations of the chain length (n = 1, 2, 3, 4, 5, 7, 9) (Fig. 10c),[69] and they reported the highest photocatalytic activity for amphiphiles with 5 and 7 methylene linkers (L5 and L7), while for L1–4 a lower TON was observed for the H_2 evolution reaction (Fig. 10e). The shorter distance for L1–4 assists electron transfer; however, the charge recombination rate was also high, and therefore low TONs were observed. The relatively high H_2 production efficiency for L5 was probably due to the molecular packing, which led to the red-shifted absorption peak and significant in phase HOMO–LUMO overlap. The author concluded that although the effect of the linker length on the photocatalytic performance was elusive, the packing and exciton splitting proficiencies have significant effects on photocatalytic performance. Later, they explored the photocatalytic H_2 gas production efficiency of electron donating and electron withdrawing group substituted perylene self-assembly (Fig. 10d and f).[56] Photocatalytic hydrogen evolution was observed for NH_2-CA and CH_3-CA self-assembly but not for CN-CA self-assembly. The lower energy offset (0.3 eV) between the LUMO of CN-CA and Mo catalyst is the probable reason for no photocatalytic activity.

Guo *et al.* explored perylene tetracarboxylic for the photocatalytic hydrogen evolution reaction (Fig. 11).[57] The presence of carboxylic groups at the periphery of the perylene core creates an internal electrical field and increases the charge carrier separation, furthermore, the photogenerated electron and hole migration to the edge and the central core, respectively, The self-assembly of perylene tetracarboxylic acid led to the formation of nanosheets with a thickness of ~1.5 nm, which is equal to the length of the PTA molecule. Hence this signifies that the 1.5 nm nanosheet consists of PTA molecules arranged based on pi–pi interaction. The ordered pi–pi stacking provides a channel for electron migration to the surface. The ultra-thin crystal plane formation inhibits the charge carrier recombination. The presence of hydrophilic groups at the periphery modulates the solubility in an aqueous medium as well as the structural engineering result in the high reduction potential required for the HER. The estimated HER for a perylene nanosheet in the presence of Pt as the co-catalyst was observed to be 118.9 mmol g^{-1} h^{-1} under irradiation of visible light (≥420 nm). The hydrogen evolution reaction was carried out for five consecutive cycles with no significant reduction in hydrogen production, demonstrating the stability and recyclability of the photocatalyst.

Zang and coworkers reported a perylene diimide derivative functionalized with either dodecyl or phenylamino groups or hetero-functionalized with dodecyl and benzyl amino groups for the formation of nanofibers.[70] The photocatalytic hydrogen evolution experiment on nanofibers with an *in situ* deposited TiO_2 layer and Pt co-catalyst showed the highest catalytic performance for the PDI with a phenyl amino group and dodecyl group attached to each end. The better photocatalytic activity for the asymmetric PDI is due to the inter- and intramolecular charge transfer. A recent review article by Sengupta *et al.* extensively reviewed the progress of perylene-based small molecules as photocatalysts for hydrogen gas evolution reactions.[71]

Other than the various photocatalysts discussed above, Cooper *et al.* reported dibenzo [b,d]thiophene sulfone and fluorene oligomers derivatives for the photocatalytic hydrogen evolution reaction. The author observed the significant impact of chain length and planarity on the photocatalytic activity.[72]

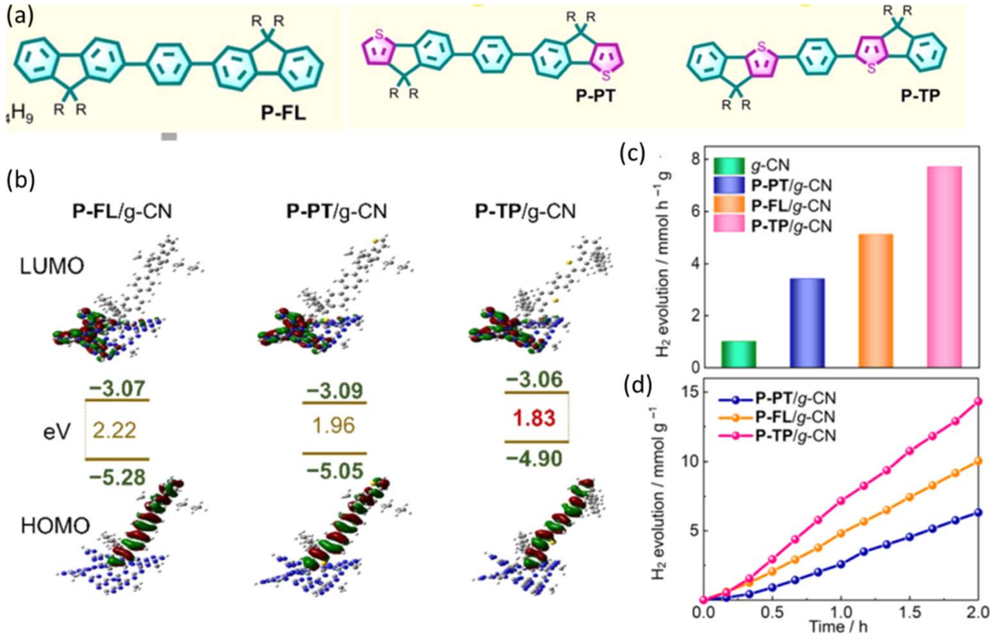

Fig. 12 (a) Chemical structure of the positional isomers. (b) DFT study for HOMO and LUMO calculation of the heterostructures. (c) P-FL/g-CN, P-PT/g-CN, P-TP/g-CN, and g-CN investigated for photocatalytic H_2 evolution rates. (d) P-FL/g-CN, P-PT/g-CN, and P-TP/g-CN studied for time-dependent photocatalytic hydrogen evolution. Reproduced with permission from ref. 58, Copyright © 2023, Royal Society of Chemistry.

2.5 Organic heterojunction nanoparticles

In a study by Long and coworkers, they reported the structural isomers with same molecular formulae but different molecular compositions which have dramatic impact on the HER.[58] They have designed two metal-free organic small molecules (OSMs) P-PT and P-TP by replacing two phenyl rings of P-FL with heterocyclic thiophene at symmetric positions and connecting the phenyl and thiophene ring with a methylene linker to inhibit free rotation (Fig. 12). The P-TP molecule was found to have better planarity in the structure compared to P-PT due to less steric hindrance induced by the small thiophene ring, which is beneficial for a fast intermolecular charge transfer process. The P-TP molecule with the alternate phenyl and thiophene rings shows that the negative charge is distributed on each phenyl ring and positive charge is localized on the upper and lower side. Whereas the P-PT derivative had negative charge in the phenyl centre and the positive charge was accumulated at both ends. Both P-TP and P-PT isomers showed good visible light-capturing ability. The author investigated the OSMs-g-CN heterostructures for the photocatalytic hydrogen gas evolution reaction. The DFT calculation for P-PT-g-CN and P-TP-g-CN heterostructures showed that the HOMO was localised on OSMs and LUMO on the graphitic carbon nitride (g-CN) centre, which facilitates effective charge transfer. The HOMO–LUMO band gap calculated for OSM-g-CN materials was observed to be 1.96 and 1.83 eV respectively for PPT-g-CN and PTP-g-CN, respectively. The photocatalytic hydrogen evolution carried out for OSMs-g-CN in aqueous solutions containing triethanolamine (TEOA), showed excellent HER for PTP-g-CN with a rate of 7.71 mmol h^{-1} g^{-1}, which is 2.26 times higher than that of P-PT/g-CN (3.41 mmol h^{-1} g^{-1}) under visible light irradiation ($\lambda > 420$ nm).

In contrast to earlier reports of single small molecule based photocatalysts for the hydrogen evolution reaction, Tian *et al.*

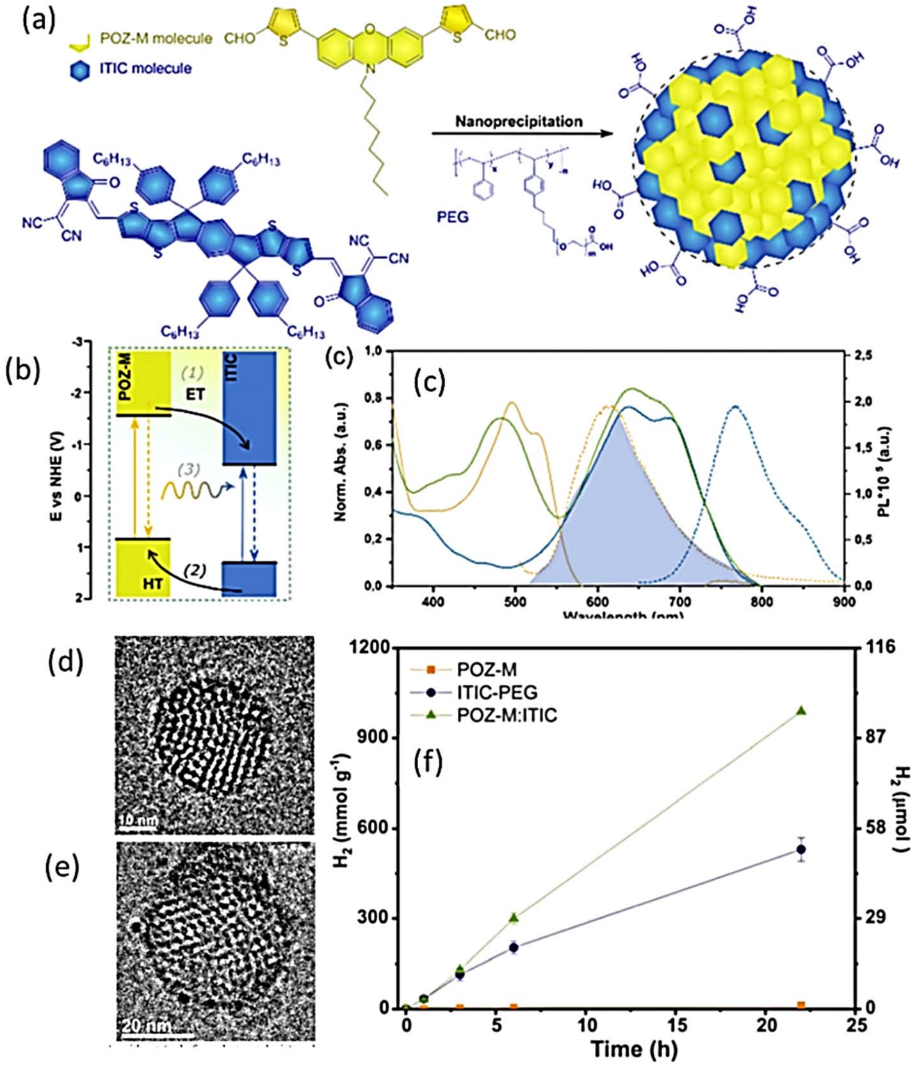

Fig. 13 (a) Schematic for preparation of NPs by nanoprecipitation from POZ-M and ITIC, (b) energy diagram for possible charge and energy transfer mechanisms, and (c) UV-vis absorption (solid lines) and emission (dashed lines) spectra of POZ-M NPs (orange), POZ-M: ITIC NPs (green) and ITIC NPs (blue) in water. Cryo-EM images of heterojunction NPs (d) before and (e) after the photocatalytic reaction and (f) photocatalytic hydrogen evolution activity for single molecule ITIC NPs (blue line), POZ-M NPs (orange line), and POZ-M: ITIC NPs (green line). Reproduced with permission from ref. 59, Copyright © 2023, Royal Society of Chemistry.

reported all-organic small molecule-based heterojunction NPs for the first time, where both the donor and acceptor are small molecules, for the photocatalytic hydrogen evolution reaction. They have reported a dithiophene substituted phenoxazine (POZ-M) small organic donor molecule for synthesis of organic donor–acceptor hetero-junction nanoparticles with small acceptor molecules (ITIC)[73] (Fig. 13).[59] The POZ-M:ITIC heterojunction nanoparticle synthesis was performed by the nanoprecipitation method with the formation of a stable NP dispersion of 30 nm diameter. While donor POZ-M exhibits absorption in the 400–570 nm range, acceptor ITIC exhibits absorption in the 520–700 nm range which is complementary to donor absorption. The powder X-ray diffraction analysis showed the crystalline nature of the co-assembly. The energy level calculation showed the staggered (type II) energy alignment of donor POZ-M and acceptor ITIC. Therefore, multiple factors contribute to the efficient charge separation *i.e.*, by electron transfer from the donor to the acceptor or hole transfer from the acceptor to the donor, energy transfer from the donor to the acceptor, and the crystalline arrangement of the donor and acceptor. Photocatalytic H_2 evolution activity of heterojunction NPs loaded with 6 wt% platinum under LED 50 mW cm^{-2} in the 420–750 nm range is equivalent to that under simulating solar light conditions, which showed a H_2 production rate of 63 mmol g^{-1} h^{-1}, which is significantly higher (2 and 100 times, respectively) than that of only ITIC NPs (29.5 mmol g^{-1} h^{-1}) and POZ-M NPs (0.6 mmol g^{-1} h^{-1}), respectively. The Cryo-EM images recorded for the heterojunction NPs 22 h after the photocatalytic activity didn't show any distinct morphology change, signifying the robustness of the system.

3 Conclusions and future perspectives

In summary, we have discussed state-of-the-art developments of molecularly engineered small molecule-based photocatalysts for green hydrogen production. We have demonstrated various classes of small molecules such as donor–acceptor, organic photovoltaic small molecules, porphyrins, perylene, and organic heterojunction nanoparticles as photocatalysts. Small molecules used in organic photovoltaics are also showing promising performance as photocatalysts for the hydrogen evolution reaction. Therefore, they have shown the potential to compete with inorganic semiconductors. The literature reports showed that structural tunability has a significant impact on the photocatalytic hydrogen evolution rate. The literature so far reported not only conjugated donor–acceptor or single small molecules as photocatalysts but also donor–acceptor heterojunction nanoparticles with good photocatalytic efficiency. The advantages of easy synthesis and structural tunability allow for intricate structural engineering to achieve outstanding photocatalytic performance.

The following conclusions can be drawn from the literature reports so far:

(a) Various structural factors play very important roles in the modulation of the photocatalytic hydrogen evolution rate. The molecules containing heteroatoms, especially nitrogen and sulfur have better photocatalytic performance. This may be because they assist in proton reduction by providing lone pair of electrons. The hetero-atom substitution decreases the HOMO and LUMO energy gap as well as increases the internal charge polarizability within the molecule, which results in the reduction of the band gap andwide absorption in the UV-vis range. Moreover, intricate control of the positioning of HOMO and LUMO energy is feasible by structural engineering for developing small molecule based efficient photocatalysts.

(b) The amphiphilic small molecules with charged functional groups have an internal electric field which facilitates charge carrier separation and reduces charge recombination, thereby favouring hydrogen evolution. The introduction of ionic functional groups at the periphery of molecules provides molecules with water solubility and dispersibility; therefore, a combination of extended pi conjugation and ionic functional group incorporation can be considered an important factor for organic small molecule based photocatalyst development.

(c) Long-range ordering and crystallinity have significant impacts on the overall photocatalytic hydrogen evolution activity. The suitable substitution on pi conjugated small molecules leads to the arrangement of small molecules in an organized fashion. Close-packed structure formation results in better donor–acceptor interaction and pi-orbital overlap, and hence improved charge carrier separation is possible. Therefore, crystal engineering can provide organic photocatalysts with superior photocatalytic activity. Various reports show that molecular packing and crystallinity have a significant impact on photocatalytic efficiency.

(d) The formation of nanoaggregates allows the organic semiconductors to undergo self-assembly with better molecular packing and more surface area, which may help in efficient exciton separation compared to bulk aggregated structures and contribute to an improved photocatalytic rate.

(e) From the reports of various groups, it can be concluded that the role of co-catalysts is not very clear. Even though most of the reports demonstrate the use of noble metals as co-catalysts, a few reports showed good photocatalytic performance in the absence of co-catalysts. Therefore, the role of a co-catalyst is still elusive and more research is required in this direction.

(f) Attempting overall water splitting to hydrogen and oxygen gas requires long-lived electrons and holes, for both reactions to proceed, which is difficult to achieve. The sacrificial reagent plays a very important role by scavenging the holes generated during photoexcitation and reducing the recombination propensity. Since the oxidation of the sacrificial reagent is thermodynamically more favourable compared to water oxidation to produce oxygen, the use of sacrificial reagents or hole scavengers enriches the photocatalyst with electrons for enhanced proton reduction. The reports so far demonstrated the important role of sacrificial reagents in the photocatalytic hydrogen evolution reaction. There are only a few reports on water splitting without the use of a sacrificial regent, and in that case, an extensive design of the photocatalytic system is required.

(g) Although different types of small molecules are showing promising activity, as well as stability under photocatalytic reaction conditions, the long-term instability of small molecules under experimental conditions by photo-oxidation limits their application. When organic molecules excited with high-intensity light irradiation there is a high chance of photobleaching and unwanted side reactions. Therefore, the exposure time to UV-visible light and intensity of radiation need to be controlled for omitting long term photo-instability.

Still, there is plenty of scope for exploration. The reports on small molecule-based photocatalysts are limited and they are still in their early stage of development. The number of small molecule photocatalysts having broad absorption in the visible range is also limited. The quantum yield of the small molecule-based photocatalyst needs to be improved to increase the PHE rate. The impact of various structural modifications on the photocatalytic hydrogen evolution rate is not well established yet. The impact of crystallinity and ordering is another area that requires much attention. One critical drawback of organic small molecule semiconductors is the high exciton binding energy that results in inefficient charge separation. Therefore, significant research is required in this direction to establish the area of organic small molecule semiconductors with better photocatalytic performance. The research on small molecules as photocatalysts for green hydrogen fuel production is growing rapidly. Additionally, organic semiconductors are being explored extensively as photocatalysts for conversion of small molecules into other fuels and they can be an attractive alternative to polymer and inorganic semiconductors for photocatalytic reactions.

Conflicts of interest

There are no conflicts to declare.

Acknowledgements

TG thanks the Department of Science and Technology (DST) for an Inspire Faculty Fellowship and research grant (DST/INSPIRE/IFF/BATCH-19/2023/IFA22-CH375). The authors also acknowledge all the researchers who contributed to the work cited in this article. CSIR-IICT Communication Number: IICT/Pubs./2024/256.

References

1 R. Zheng, Z. Liu, Y. Wang, Z. Xie and M. He, *Joule*, 2022, **6**, 1148–1159.
2 P. Poizot and F. Dolhem, *Energy Environ. Sci.*, 2011, **4**, 2003–2019.
3 N. L. Panwar, S. C. Kaushik and S. Kothari, *Renewable Sustainable Energy Rev.*, 2011, **15**, 1513–1524.
4 A. Midilli, I. Dincer and M. Ay, *Energy Policy*, 2006, **34**, 3623–3633.
5 H. Tan, J. Li, M. He, J. Li, D. Zhi, F. Qin and C. Zhang, *J. Environ. Manage.*, 2021, **297**, 113382.
6 I. Gunnarsdottir, B. Davidsdottir, E. Worrell and S. Sigurgeirsdottir, *Renewable Sustainable Energy Rev.*, 2021, **141**, 110770.
7 X. Chen, S. Shen, L. Guo and S. S. Mao, *Chem. Rev.*, 2010, **110**, 6503–6570.
8 I. Staffell, D. Scamman, A. Velazquez Abad, P. Balcombe, P. E. Dodds, P. Ekins, N. Shah and K. R. Ward, *Energy Environ. Sci.*, 2019, **12**, 463–491.
9 P. J. Megia, A. J. Vizcaino, J. A. Calles and A. Carrero, *Energy and Fuels*, 2021, **35**, 16403–16415.
10 Z. J. Baum, L. L. Diaz, T. Konovalova and Q. A. Zhou, *ACS Omega*, 2022, **7**, 32908–32935.
11 M. Z. Rahman, M. G. Kibria and C. B. Mullins, *Chem. Soc. Rev.*, 2020, **49**, 1887–1931.
12 S. Chen, T. Takata and K. Domen, *Nat. Rev. Mater.*, 2017, **2**, 17050.
13 H. Song, S. Luo, H. Huang, B. Deng and J. Ye, *ACS Energy Lett.*, 2022, **7**, 1043–1065.
14 A. Fujishima and K. Honda, *Nature*, 1972, **238**, 37–38.
15 A. Fujishima, K. Kohayakawa and K. Honda, *J. Electrochem. Soc.*, 1975, **122**, 1487–1489.
16 K. Maeda, *J. Photochem. Photobiol., C*, 2011, **12**, 237–268.
17 G. Colón, *Appl. Catal., A*, 2016, **518**, 48–59.
18 A. A. Ismail and D. W. Bahnemann, *Sol. Energy Mater. Sol. Cells*, 2014, **128**, 85–101.
19 Y. J. Yuan, Z. T. Yu, D. Q. Chen and Z. G. Zou, *Chem. Soc. Rev.*, 2017, **46**, 603–631.
20 Y. Bai, Z. Hu, J. X. Jiang and F. Huang, *Chem. - Asian J.*, 2020, **15**, 1780–1790.
21 Y. Bai, C. Li, L. Liu, Y. Yamaguchi, M. Bahri, H. Yang, A. Gardner, M. A. Zwijnenburg, N. D. Browning, A. J. Cowan, A. Kudo, A. I. Cooper and R. S. Sprick, *Angew. Chem., Int. Ed.*, 2022, **61**, e202201299.
22 H. Yang, X. Li, R. S. Sprick and A. I. Cooper, *Chem. Commun.*, 2020, **56**, 6790–6793.
23 Z. Yu, X. Yue, J. Fan and Q. Xiang, *ACS Catal.*, 2022, **12**, 6345–6358.
24 A. Naseri, M. Samadi, A. Pourjavadi, A. Z. Moshfegh and S. Ramakrishna, *J. Mater. Chem. A*, 2017, **5**, 23406–23433.
25 X. Chu, C. I. Sathish, J.-H. Yang, X. Guan, X. Zhang, L. Qiao, K. Domen, S. Wang, A. Vinu and J. Yi, *Small*, 2023, **19**, 2302875.
26 Y. Li, X. Song, G. Zhang, L. Wang, Y. Liu, W. Chen and L. Chen, *ChemSusChem*, 2022, **15**, e202200901.
27 T. Banerjee, K. Gottschling, G. Savasci, C. Ochsenfeld and B. V. Lotsch, *ACS Energy Lett.*, 2018, **3**, 400–409.
28 Y. Wang, A. Vogel, M. Sachs, R. S. Sprick, L. Wilbraham, S. J. A. Moniz, R. Godin, M. A. Zwijnenburg, J. R. Durrant, A. I. Cooper and J. Tang, *Nat. Energy*, 2019, **4**, 746–760.
29 S. Cao, L. Piao and X. Chen, *Trends Chem.*, 2020, **2**, 57–70.
30 Y. Inoue, *Energy Environ. Sci.*, 2009, **2**, 364–386.
31 A. B. Suman, R. Datt, V. Gupta and S. P. Singh, *Chem. Commun.*, 2017, **53**, 12790–12793.
32 P. Murugan, T. Hu, X. Hu and Y. Chen, *J. Mater. Chem. A*, 2022, **10**, 5044–5081.
33 Y. S. Yen, H. H. Chou, Y. C. Chen, C. Y. Hsu and J. T. Lin, *J. Mater. Chem.*, 2012, **22**, 8734–8747.

34 A. Siddiqui, N. Islavath, T. Swetha and S. P. Singh, *Energy Adv.*, 2023, **2**, 1045–1050.

35 P. Y. Gu, N. Wang, C. Wang, Y. Zhou, G. Long, M. Tian, W. Chen, X. W. Sun, M. G. Kanatzidis and Q. Zhang, *J. Mater. Chem. A*, 2017, **5**, 7339–7344.

36 T. H. Schloemer, J. A. Christians, J. M. Luther and A. Sellinger, *Chem. Sci.*, 2019, **10**, 1904–1935.

37 C. Rodríguez-Seco, L. Cabau, A. Vidal-Ferran and E. Palomares, *Acc. Chem. Res.*, 2018, **51**, 869–880.

38 C. P. Lee, C. T. Li and K. C. Ho, *Mater. Today*, 2017, **20**, 267–283.

39 K. S. Yook and J. Y. Lee, *Adv. Mater.*, 2014, **26**, 4218–4233.

40 K. Narayanaswamy, A. Venkateswararao, V. Gupta, S. Chand and S. P. Singh, *Chem. Commun.*, 2016, **52**, 210–213.

41 L. Giribabu, N. Duvva, S. Prasanthkumar, S. P. Singh, L. Han, I. Bedja, R. K. Gupta and A. Islam, *Sustainable Energy Fuels*, 2017, **1**, 345–353.

42 Y. Chen, C. Yan, J. Dong, W. Zhou, F. Rosei, Y. Feng and L. N. Wang, *Adv. Funct. Mater.*, 2021, **31**, 2104099.

43 J. Kosco, F. Moruzzi, B. Willner and I. McCulloch, *Adv. Energy Mater.*, 2020, **10**, 2001935.

44 Y. Wang, F. Silveri, M. K. Bayazit, Q. Ruan, Y. Li, J. Xie, C. R. A. Catlow and J. Tang, *Adv. Energy Mater.*, 2018, **8**, 1801084.

45 Y. Guo, Q. Zhou, B. Zhu, C. Y. Tang and Y. Zhu, *EES Catal.*, 2023, **1**, 333–352.

46 X. Yuan, C. Wang, L. Vallan, A. T. Bui, G. Jonusauskas, N. D. McClenaghan, C. Grazon, S. Lacomme, C. Brochon, H. Remita, G. Hadziioannou and E. Cloutet, *Adv. Funct. Mater.*, 2023, **33**, 2211730.

47 J. Yu, S. Chang, X. Xu, X. He and C. Zhang, *ACS Sustain. Chem. Eng.*, 2020, **8**, 14253–14261.

48 G. Zhang, X. Yang, Y. Li, P. Zhang and H. Mi, *ChemSusChem*, 2019, **12**, 5070–5074.

49 Y. Wan, J. Deng, C. Gu and Y. Ma, *J. Mater. Chem. A*, 2021, **9**, 2120–2125.

50 Y. Zhu, Z. Zhang, W. Si, Q. Sun, G. Cai, Y. Li, Y. Jia, X. Lu, W. Xu, S. Zhang and Y. Lin, *J. Am. Chem. Soc.*, 2022, **144**, 12747–12755.

51 Y. Liang, T. Li, Y. Lee, Z. Zhang, Y. Li, W. Si, Z. Liu, C. Zhang, Y. Qiao, S. Bai and Y. Lin, *Angew. Chem., Int. Ed.*, 2023, **62**, e202217989.

52 Y. Li, Z. Zhang, T. Li, Y. Liang, W. Si and Y. Lin, *Angew. Chem., Int. Ed.*, 2023, **62**, e202307466.

53 H. Li, L. Jie, J. Pan, L. Kang and J. Yao, *J. Mater. Chem. A*, 2016, **4**, 6577–6584.

54 X. Yang, Z. Hu, Q. Yin, C. Shu, X.-F. Jiang, J. Zhang, X. Wang, J.-X. Jiang, F. Huang and Y. Cao, *Adv. Funct. Mater.*, 2019, **29**, 1808156.

55 A. S. Weingarten, R. V. Kazantsev, L. C. Palmer, M. McClendon, A. R. Koltonow, A. P. S. Samuel, D. J. Kiebala, M. R. Wasielewski and S. I. Stupp, *Nat. Chem.*, 2014, **6**, 964–970.

56 A. S. Weingarten, A. J. Dannenhoffer, R. V. Kazantsev, H. Sai, D. Huang and S. I. Stupp, *J. Am. Chem. Soc.*, 2018, **140**, 4965–4968.

57 Y. Guo, Q. Zhou, J. Nan, W. Shi, F. Cui and Y. Zhu, *Nat. Commun.*, 2022, **13**, 2067.

58 Q. Zhang, D. Li, Z. Zhao, K. Zheng, Q. Wang, B. Wang and X. Long, *J. Mater. Chem. A*, 2023, **11**, 5937–5944.

59 M. V. Pavliuk, S. Wrede and H. Tian, *Chem. Commun.*, 2023, **59**, 5611–5614.

60 X. Yuan, K. Yang, C. Grazon, C. Wang, L. Vallan, J.-D. Isasa, P. M. Resende, F. Li, C. Brochon, H. Remita, E. Hadziioannou, G. Cloutet and J. Li, *Angew. Chem., Int. Ed.*, 2024, **63**, e202315333.

61 C. Li, J. Zhou, J. Song, J. Xu, H. Zhang, X. Zhang, J. Guo, L. Zhu, D. Wei, G. Han, J. Min, Y. Zhang, Z. Xie, Y. Yi, H. Yan, F. Gao, F. Liu and Y. Sun, *Nat. Energy*, 2021, **6**, 605–613.

62 J. Wang, P. Xue, Y. Jiang, Y. Huo and X. Zhan, *Nat. Rev. Chem*, 2022, **6**, 614–634.

63 Z. Zheng, J. Wang, P. Bi, J. Ren, Y. Wang, Y. Yang, X. Liu, S. Zhang and J. Hou, *Joule*, 2022, **6**, 171–184.

64 S. Kraner, R. Scholz, C. Koerner and K. Leo, *J. Phys. Chem. C*, 2015, **119**, 22820–22825.

65 Z. Zhang, W. Si, B. Wu, W. Wang, Y. Li, W. Ma and Y. Lin, *Angew. Chem.*, 2022, **61**, e202114234.

66 Z. Zhang, Y. Zhu, X. Chen, H. Zhang and J. Wang, *Adv. Mater.*, 2019, **31**, 1806626.

67 C. F. N. Marchiori, G. B. Damas and C. M. Araujo, *J. Power Sources Adv.*, 2022, **15**, 100090.

68 A. D. Wilson, R. K. Shoemaker, A. Miedaner, J. T. Muckerman, D. L. DuBois and M. R. DuBois, *Proc. Natl. Acad. Sci. U. S. A.*, 2007, **104**, 6951–6956.

69 A. S. Weingarten, R. V. Kazantsev, L. C. Palmer, D. J. Fairfield, A. R. Koltonow and S. I. Stupp, *J. Am. Chem. Soc.*, 2015, **137**, 15241–15246.

70 S. Chen, D. L. Jacobs, J. Xu, Y. Li, C. Wang and L. Zang, *RSC Adv.*, 2014, **4**, 48486–48491.

71 A. Kumari and S. Sengupta, *ChemCatChem*, 2024, **16**, e202301033.

72 C. M. Aitchison, M. Sachs, M. A. Little, L. Wilbraham, N. J. Brownbill, C. M. Kane, F. Blanc, M. A. Zwijnenburg, J. R. Durrant, R. S. Sprick and A. I. Cooper, *Chem. Sci.*, 2020, **11**, 8744–8756.

73 A. Liu, L. Gedda, M. Axelsson, M. Pavliuk, K. Edwards, L. Hammarström and H. Tian, *J. Am. Chem. Soc.*, 2021, **143**, 2875–2885.